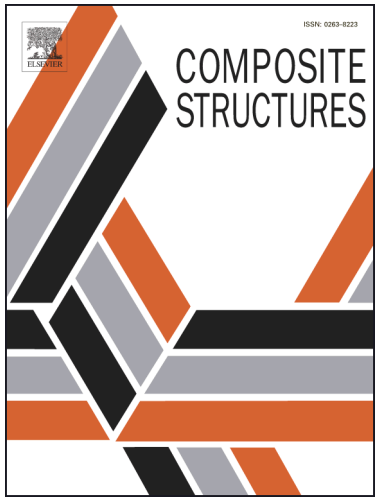

Design and analysis of shockless smart releasing device based on shape memory polymer composites

Hanxing Zhao, Xin Lan, Liwu Liu, Yanju Liu, Jinsong Leng

PII: S0263-8223(18)34257-0
DOI: https://doi.org/10.1016/j.compstruct.2019.110958
Article Number: 110958
Reference: COST 110958

To appear in: *Composite Structures*

Received Date: 26 November 2018
Revised Date: 18 March 2019
Accepted Date: 2 May 2019

Please cite this article as: Zhao, H., Lan, X., Liu, L., Liu, Y., Leng, J., Design and analysis of shockless smart releasing device based on shape memory polymer composites, *Composite Structures* (2019), doi: https://doi.org/10.1016/j.compstruct.2019.110958

Design and analysis of shockless smart releasing device based on shape memory polymer composites

Hanxing Zhao[1], Xin Lan[1], Liwu Liu[2], Yanju Liu[2], Jinsong Leng[1]*

[1] National Key Laboratory of Science and Technology on Advance Composites in Special Environments, Science Park of Harbin Institute of Technology (HIT), Harbin 150080, China

[2] Department of Astronautical Science and Mechanics, Harbin Institute of Technology, Harbin 150001, China

*Au to whom correspondence should be addressed. Tel. /FAX: +86-451-86403269. Electronic mail: lengjs@hit.edu.cn

Abstract: In this paper, a new releasing device with the advantages of non-pyrotechnic, shockless, re-settable, and simple structured are presented. A sandglass-like mechanism is designed and it is made of carbon fiber reinforced epoxy-based shape memory polymer (SMP) and its composite (SMPC). The SMPC active element is the outer part, while the inner part is made of metal with a sandglass-like profile. The active element is designed to change shape and accomplish a separation between the mating parts of the release mechanism with no impact. The actuation of the SMPCs parts is not an instant but duration, so that the considerable preload will be released gently and with no impacting shock. Some basic mechanical tests for SMP and SMPC plate specimens were done to determine the basic mechanical properties of the epoxy-based SMP and SMPC. The locking-compression test, axial tensile test and relaxation test were conducted to determine the mechanical properties of the smart releasing device. The recovery experiment of the device was also applied and the scanning electron microscope (SEM) was used to observe the morphologies of the SMPC cylinders of the smart releasing devices before and after releasing.

Keywords: composite, smart releasing device, shape memory polymer

1.Introduction

Shape memory polymer (SMP) have the ability to respond to external stimulus (e.g., heat, light, electric field, magnetic field, moisture and PH changing) and deform from the temporary shape to its original shape [1-6]. The shape memory mechanism of SMP can be described as follows: (a) When a SMP specimen is heated above its glass transition temperature (Tg), it will change from hard to soft. (b) An external force is applied, and the specimen can be bended to a temporary state. (c) The applied force remains constant during the cooling process. (d) After the external force is removed, the shape of the specimen can remain unchanged. (e) When the specimen is imposed to external stimuli, the temporary shape can recover to the original shape [7]. The above shape memory process of SMP is repeatable [7]. SMPs have the advantages of being lower cost, lighter weight, easier handling and larger deformability compared with the shape memory alloys (SMAs) [8-10]. As an advanced material, SMPs have been widely used in aerospace especially as deployable structures in spacecrafts [27]. However, the low strength and low stiffness of SMPs are also can't be neglected, so some particles or fiber fillers are added as the reinforcing materials [12-15]. Carbon fibers are one type of ideal reinforcement, mainly for its low density, high modulus, high thermal stability and chemical resistant property [15-18]. Therefore, the applications of shape memory polymer composites (SMPCs) are widely investigated, such as SMPC hinges, SMPC booms, solar arrays and so on [19-25].

With the rapid development of space technology, a variety of releasing devices are required by spacecrafts to accomplish separating the launch vehicles from the appendages [26]. Various kinds of releasing devices are reported with different forms and power sources [27-29]. The pyrotechnic releasing devices are the most traditional and most common devices among all kinds of releasing devices, but when compared with the non-powder devices, high shock and environmental pollution are the mainly limiting factors for application [45-47]. In recent years, some promising solutions have been proposed, for example, SMAs and SMPs releasing devices are developed [30-35]. The stockless thermally Actuated Release Nut (Star Nut) made of Elastic Memory Composite (EMC) reinforced by cross-ply fibers was presented by Keith in 2003 [36]. The Star Nut had the advantages of being light weight and low cost compared with the SMA releasing devices [36]. However, the locking capacity and the releasing time of the Star Nut were not mentioned. Hereafter, Leng, *et al*. designed a kind of "eight paws" smart releasing device in 2015 and tested the tensile property and the deformation recovery property of it [37]. The recovery time of the "eight paws" device is about 30s and recovery temperature is about 67℃.

In this work, we designed a "sand clock" form smart releasing device, and the outer shell of the device was made of SMPs or SMPCs cylinder. This work used liquid resin infusion method and filament winding process to fabricate the SMPs and SMPCs releasing devices, respectively. The shape memory epoxy resin and carbon fiber were used as the matrix and the reinforcement, respectively. A simplified model was proposed to preliminary study the relationship between axial tensile force and the pressure applied by the inner core. Compared with the Star Nut, the locking capacity

and the releasing time were investigated in this research. Furthermore, the locking capacity was almost 10 times larger than that of the "eight paws" device as mentioned before. Moreover, relaxation experiment of this smart releasing device was done to determine its mechanical properties after a long period of load bearing.

2.Design of the smart releasing device

This paper presents a kind of "sand clock" form shockless smart releasing device as shown in Fig. 1 and Fig. 2, the outer cylinder is made of SMP or SMPC, while the inner core is made of iron. The inner core is designed as a "sand clock" form to provide sufficient locking force for the device. The relevant characteristics of the cylinders are listed in Table 1, meanwhile the preliminary demands of smart releasing device are listed in Table 2. The different cylinder length was used for SMP (120mm) and SMPC (150mm) because during our following axial tensile test, the number of grooves of the SMPC devices was chosen to be 1, 2 and 3, but the groove's number of the SMP devices was only 2. So, the SMPC cylinder needs to be longer than SMP cylinder.

The working process of the SRD is as follows: Firstly, the outer cylinder and the inner core were assembled as shown in Fig. 1(a). Secondly, the device was placed in an oven at 100℃ for 30minutes to ensure it to be heated evenly. The cylinder will become soft enough to undergo great distortion without breaking, as shown in Fig. 1(b). Then, the cylinder was compressed by specially-made compression clamps after the device was taken out from the oven immediately, as shown in Fig. 1(c). The clamp was installed in a Zwick Z050 testing machine and the testing machine can provide uniform pressure. Afterwards, the clamps were kept still until the whole cylinder was naturally cooled down to the room temperature, as shown in Fig. 1(d). So far, the locking process had been completed. When releasing process was required, the device was reheated and the outer cylinder will recover to its initial state, so that the device can release easily, as shown in Fig. 1(e).

The device would not always be heated in an oven if it is used in the real application, so a heating strategy must be proposed. As shown in Fig. 1(f), a heating rod was used to heat the inner core. When the releasing devices need to be heated, the heating rod can heat the inner core, so that the outer cylinder can be heated by heat conduction. The actuation of the SMPCs parts is not an instant but duration, so that the considerable preload will be released slowly and with extremely low or even no impacting shock. In addition, the loading capacity and releasing time can be adjusted via changing the number and depth of the grooves.

3. Mechanical Analysis of smart releasing device

Several analyses are performed in order to better evaluate the mechanical properties of the smart releasing device during the axial tension test. The SMPC cylinder is simplified as shown in Fig. 3. The outer cylinder is assumed to be fitted together closely with the inner core (i.e., conical), and the pressure applied by the inner core during the

axial tensile process is assumed to be uniformly. F_{axial} is the axial tensile force, r and t are the diameter and thickness of the SMPC cylinder, ε_{cir} is the maximal circumferential strain of the outer cylinder during the locking process, thus the minimum diameter of the cylinder is $r(1-\varepsilon_{cir})$. So, the resultant average internal axial and circumferential stressed are:

$$\sigma_{axial} = \frac{F_{axial}}{2\pi rt} \tag{1}$$

$$\sigma_{cir} = \frac{F_{axial}}{2\pi rt\varepsilon_{cir}} \tag{2}$$

It is obvious that $\sigma_{cir} = \sigma_{axial}/\varepsilon_{cir}$, and if ε_{cir} is relatively small, σ_{cir} is much larger than the σ_{axial}, and σ_{cir} is the main factor to be considered in the design process. The experimental results also show that with the increase of the tensile load, the SMPC grooves gradually been stretched, so the circumferential stress dominates the stress condition of an axially loaded, swaged cylinder. Thus, when the smart releasing device is applied to tensile force, the axial stress can be ignored but only consider the uniform pressure which is applied by the inner core.

As for the inner core of general axisymmetric shape (not always conical shape), the above calculation method still has some deficiencies. What's more, the fiber winding angle should also be considered, so an analysis methodology which is based on film theory and classical laminate theory (CLT) is proposed to evaluate the radial strain and stress of fiber winding axisymmetric structure with different winding angles under different internal pressures. This calculation method proposed in this paper is expected to lay a foundation for our future work, so we just derived the formula but didn't compute it. Some assumptions should be made before building the theoretical model:

(a) The deformed SMPC cylinder and its lamina are in the generalized plane stress condition.

(b) Ignore the effect of the bending and torsion stiffness of the SMPC cylinder.

So, fiber winding structure is considered to be thin film, that is to say: the fiber winding cylinder is simplified into an axisymmetric shell structure in the generalized plane stress condition, and its typical geometrical shape and coordinate system as shown in Fig. 4.

θ and s are the meridian and circumferential directions, respectively. The angle φ is the colatitude angle. The meridian s, the tangent line of θ and the normal of the cylinder shell η form the local reference rectangular coordinate system (s, θ, η).

According to thin film theory [41], thin film's internal force of general axisymmetric shell is:

$$N_s = \frac{1}{r_\theta sin^2\varphi}\int_{\varphi_0}^{\varphi}\left(p_\eta cot\varphi - p_s\right) r_s r_\theta sin^2\varphi d\varphi \tag{3}$$

$$N_\theta = r_\theta\left(p_\eta - \frac{N_s}{r_s}\right) \tag{4}$$

$$N_{\theta s} = N_{s\theta} = 0 \tag{5}$$

Where p_s and p_η are the unit load of meridian and normal directions, respectively. Because we only consider the uniform normal pressure applied by the inner core. So $p_s = 0,\ p_\eta = con$, and the above formula can be simplified as:

$$N_s = \frac{1}{2} p_\eta r_\theta \left(1 - \frac{r_0^2}{r^2}\right) \tag{6}$$

$$N_\theta = \frac{1}{2} p_\eta r_\theta \left[2 - \frac{r_\theta}{r_s}\left(1 - \frac{r_0^2}{r^2}\right)\right] \tag{7}$$

$$N_{\theta s} = N_{s\theta} = 0 \tag{8}$$

Where x is the axial coordinate of the axisymmetric shell; r and r_0 are the maximum radius and minimum radius of the axisymmetric shell, respectively; r_s and r_θ are the meridian and circumferential radius of curvatures, respectively. And the expressions of r_s and r_θ are:

$$r_s = \frac{\sqrt{\left[1+\left(\frac{\partial r}{\partial x}\right)^2\right]^3}}{\frac{\partial^2 r}{\partial x^2}} \tag{9}$$

$$r_\theta = r\sqrt{1 + \left(\frac{\partial r}{\partial x}\right)^2} \tag{10}$$

It is noteworthy that the above formulas are derived from equilibrium condition, which is independent with the material properties of the shell. But the effect of fiber winding angle on the carrying capacities of the smart releasing device should also be considered. According to the classical laminate theory (CLT), the relationship between axial stress and strain of a lamina is:

$$\begin{Bmatrix}\sigma_1\\ \sigma_2\\ \sigma_3\end{Bmatrix} = \begin{bmatrix}Q_{11} & Q_{12} & 0\\ Q_{21} & Q_{22} & 0\\ 0 & 0 & Q_{66}\end{bmatrix}\begin{Bmatrix}\varepsilon_1\\ \varepsilon_2\\ \gamma_{12}\end{Bmatrix} \tag{11}$$

Where **Q** is the stiffness matrix of the SMPC, which can be expressed as follow:

$$Q_{11} = \frac{E_1}{1-\nu_{12}\nu_{21}} \tag{12}$$

$$Q_{22} = \frac{E_2}{1-\nu_{12}\nu_{21}} \tag{13}$$

$$Q_{12} = Q_{21} = \frac{\nu_{21}E_2}{1-\nu_{21}\nu_{12}} = \frac{\nu_{12}E_1}{1-\nu_{21}\nu_{12}} \tag{14}$$

$$Q_{66} = G_{12} \tag{15}$$

And **ε** is the strain matrix, which can be derived from the formula of rotated axes:

$$\begin{Bmatrix}\varepsilon_1\\ \varepsilon_2\\ \gamma_{12}\end{Bmatrix} = \begin{bmatrix}1 & \cos 2\alpha & \sin 2\alpha\\ 1 & -\cos 2\alpha & -\sin 2\alpha\\ 0 & -2\sin 2\alpha & 2\cos 2\alpha\end{bmatrix}\begin{Bmatrix}\frac{1}{2}(\varepsilon_s + \varepsilon_\theta)\\ \frac{1}{2}(\varepsilon_s - \varepsilon_\theta)\\ \frac{1}{2}\gamma_{s\theta}\end{Bmatrix} \tag{16}$$

Where α is the fiber winding angle. ε_s and ε_θ are the meridian and circumferential strain of the shell, respectively, which is given by the thin film constitutive equation [42,43]:

$$\begin{Bmatrix} N_s \\ N_\theta \end{Bmatrix} = \begin{bmatrix} U_1 + U_4 + U_2V_1 & U_1 - U_4 + U_2V_1 + 2U_3V_2 \\ U_1 + U_4 - U_2V_1 & U_4 - U_1 + U_2V_1 - 2U_3V_2 \end{bmatrix} \begin{Bmatrix} \frac{1}{2}(\varepsilon_s + \varepsilon_\theta) \\ \frac{1}{2}(\varepsilon_s - \varepsilon_\theta) \end{Bmatrix} \tag{17}$$

Where U_1, U_2, U_3 and U_4 are stiffness invariant:

$$U_1 = \frac{1}{4}[Q_{11} + 2(Q_{12} + 2Q_{66}) + Q_{22}] \tag{18}$$

$$U_2 = \frac{1}{2}(Q_{11} - Q_{22}) \tag{19}$$

$$U_3 = \frac{1}{4}[Q_{11} - 2(Q_{12} + 2Q_{66}) + Q_{22}] \tag{20}$$

$$U_4 = \frac{1}{4}[Q_{11} + 2(Q_{12} - 2Q_{66}) + Q_{22}] \tag{21}$$

The geometrical factors V_1 and V_2 are:

$$V_1 = \frac{1}{h}\int_0^1 \cos 2\alpha(u)\, du \tag{22}$$

$$V_2 = \frac{1}{h}\int_0^1 \cos^2 2\alpha(u)\, du \tag{23}$$

Where $\alpha(u)$ is fiber angle along the direction of shell's thickness, h is the thickness of the shell. Substitute the stiffness invariant U_1, U_2, U_3, U_4 and the geometrical factors V_1, V_2 into the thin film constitutive equation, the relationship between stress, strain and displacement of corresponding shell can be found out.

According to Giles [44], the meridian and circumferential strain of the fiber winding axisymmetric shell are:

$$\varepsilon_s = \frac{1}{r_s}\left(\frac{\partial u}{\partial \varphi} + w\right) \tag{24}$$

$$\varepsilon_\theta = \frac{1}{r_\theta}(u\cot\varphi + w) \tag{25}$$

Then the meridian and circumferential displacements of the fiber winding axisymmetric shell can be derived according to equations (16) and (24) and (25):

$$u = \sin\varphi\left(\int \frac{r_s\varepsilon_s - r_\theta\varepsilon_\theta}{\sin\varphi}\right)d\varphi + C_1 \tag{26}$$

$$w = r_\theta\varepsilon_\theta - u\cot\varphi \tag{27}$$

When $\varphi = \frac{\pi}{2}$,u $= 0$, so the integration constant C_1 can be determined.

The uniform internal pressure is supposed to be $p_\eta = 1$MPa, a: b: $r_0 = 20:12:5$, E_1, E_2, v_{12} and G_{12} are the material performance of common carbon fiber composite: $E_1 = 142$GPa, $E_2 = 10.8$GPa, $v_{12} = 0.3$ and $G_{12} = 5.49$GPa. Using the above formulas, the analysis results are shown in Fig. 5. There are two implications:

(1) The longitudinal film stress of the shell decreases sharply near the opening of the shell.

(2) The radical displacement, transverse and shear stress of the shell are all negative values near the equator of the shell, and they all change dramatically.

Using the above-mentioned formulas, the relationship between stress, strain and displacement of SMPC cylinder can be determined. Meanwhile, the relationship between axial tensile force and the pressure applied by the inner core can be expressed in terms of force balance expression. Thus, this calculation method proposed in this paper have some instructive meanings when investigating the mechanical properties of the smart releasing device during the axial tension test.

4. Experiments

4.1 Materials preparation

The materials used in this article were shape memory epoxy resin and its composites. The polymer matrix was synthesized by Leng, *et al.* [4] and T700 Toray carbon fibers were used as the reinforcement. The mold as shown in Fig. 6 was designed to fabricate the outer SMP cylinder by liquid resin infusion method. The mold was made of the polytetrafluoroethylene (PTEF), which is an ideal material to be demolded easily. An autoclave was used to cure the resin after the epoxy resin was infused into the mold. Curing process was set into three steps: 80℃ for 3 h, 100℃ for 3 h and 150℃ for 5 h. The outer SMPC cylinder was fabricated by filament winding process and cured by the same curing process. The volume fraction of carbon fiber was approximately 60%, while the winding angle was 45°. Both the SMP and SMPC outer cylinders were 2mm thick, and the inner diameter was 36mm.

In order to determine the mechanical properties of the materials, pure shape memory epoxy resin and its composites flat plat specimens were also fabricated, using liquid resin infusion and filament winding methods, respectively. The SMP and SMPC specimens were cut for dynamic mechanical analyzer (DMA) test, tension test and shape memory property test.

4.2 Characterization methods of flat plat specimens

In order to determine the basic mechanical properties of the epoxy resin-based SMP and SMPC, the following characterizations are conducted: DMA test, isothermal uniaxial tension test and shape memory behavior test [38-40]. The SMP and SMPC plates are cut into appropriate size by a CNC engraving and milling machine.

4.2.1 Mechanical test for the epoxy-based SMP and SMPC

The viscoelastic characteristics of polymer are defined as that the modulus are composed of two parts, one is the storage modulus evaluating elasticity of material, and the other part is the loss modulus evaluating viscosity of material. For viscoelastic materials, the strain is behind a phase angle of stress, which can be expressed as loss factor, and it equals to loss modulus divided by storage modulus. In order to identify the glass transition temperature (Tg) and the dynamic thermomechanical properties of the specimens, DMA test was performed by a TA instrument DMA Q800 machine. In the DMA test, the epoxy-based SMPs and SMPCs were incised into rectangular

specimens with dimension of 35mm×5mm×2mm according to ASTM D5023. The experiment parameters were specified as: a multi frequency mode and the frequency was chosen to be 1.0 Hz; the heating rate was chosen to be $5℃/\mathrm{min}$; the temperature range was $25℃\sim150℃$ and using the three-point bending clamp arrangement.

Isothermal uniaxial tension test was conducted in a universal mechanical test instrument (Zwick Z050) with a loading rate of 2mm/min, under different temperature conditions ($25℃,\ 60℃,\ 80℃, 100℃,$ and $120℃$). In the isothermal uniaxial tension test, the epoxy-based SMPs were incised into Dumbbell-shape Type V specimens according to ASTM D638, while the epoxy-based SMPCs were incised into rectangular specimens with dimension of 250mm×25mm×2.5mm according to ASTM D3039. Five specimens were prepared for each test conditions, and the experimental results were expressed by the mean value of the experimental data.

4.2.2 Shape memory property test for the epoxy-based SMP and SMPC

A special shape memory mold was fabricated as illustrated in Fig. 7(a), and the following steps were taken to calculate the retention and recovery ratios of the SMP or SMPC specimens: (1) the specimens were placed in an oven to heat up to 120℃ and held for 10min; (2) after the specimens were soft enough, they were bended by the mold into "U" shape, as shown in Fig. 7(a) and Fig. 7(b), then it was cooled down to the room temperature. (3) the "U" shape specimens were taken out from the mold, and the bending angle θ_{fixed} was measured as shown in Fig. 7(c). (4) all specimens were heated again in order to recover the initial shape of the specimens, and the corresponding bending angle θ_{re} was measured too, as shown in Fig. 7(d). Moreover, when the specimens were reheated, the recovered time t_{re} was also recorded to obtain the recovery rate.

Shape retention ratio: $R_f = \frac{180°-\theta_{fixed}}{180°} \times 100\%$ (28)

Shape recovery ratio: $R_r = \frac{180°-\theta_{re}}{180°} \times 100\%$ (29)

Shape recovery rate: $V_r = \frac{(180°-\theta_{re}-\theta_{fixed})}{t_{re}}$ (30)

4.3 Characterization methods of smart releasing devices

The locking compression test, axial tensile test and relaxation test were conducted to evaluate the mechanic properties of the smart releasing devices. As shown in Fig. 6, the locking compression test and axial tensile test were carried out on a Zwick Z050 testing machine, while the relaxation test was processed on a creep testing machine. The releasing actuation time was also the point we concerned, therefore the recovery experiment of the devices was applied. Furthermore, the SEM was used to observe the morphologies of the SMPC cylinders of the smart releasing devices before and after releasing.

4.3.1 Locking compression test

In order to know the relationship between the compressive force and the depth of

groove, the locking compression test was done as shown in Fig. 8(b). The SMPC devices were placed in the middle of the clamp after taking out of the oven. When the compressive test went on, the cylinder was heated by a heat gun to make sure the temperature of the outer cylinder was above its Tg all the time. For better comparison, the test of the device without the inner core was also conducted.

4.3.2 Axial tensile test

Carrying capacity is one of the most significant technology indicators for the releasing device in this study, so various axial tensile tests with different number of grooves and different depth of the grooves are done to confirm the influencing factors of the carrying capacity. Table 3 lists the serial number of the tensile test under different conditions, all specimens are tested as shown in Fig. 8(a). The tensile speed and the environment temperature are set to 2mm/min and 25℃, respectively.

4.3.3 Relaxation test

The launch vehicles may stay for a long period of time in space, during the locking duration, the appendages must be locked tightly. If there is a significant drop of the locking force, some bad effects may occur on the spacecrafts. So, it is advisable to study the residue locking force of the releasing devices in stretched form after a period of time. Therefore, as shown in Fig. 8(c), the relaxation test is carried out to research the force relaxation phenomenon of the releasing device.

4.3.4 Recovery test

The actuated time is also an important indicator to measure the performance of the releasing device because fast actuation capacity is always required in the aerospace field. A camera is used to record the releasing process of the device. There are many methods to heat the outer cylinder of the device. To simplify the operation, an oven with a transparent door is chosen as a heating source. After preheating the oven to 100℃, the device was put into the oven meanwhile the whole recovery process was recorded by a camera until the grooves were flattened completely.

4.3.5 Morphology test

The SMPC cylinders will inevitably suffer different degrees of damage after the SRDs are locked and released, which may be hard to observe by eyes. Therefore, the SEM is used to observe the morphologies of the SMPC cylinders before and after releasing. SMPC2-10, SMPC2-12 and SMPC2-14 are selected to find out the influence on the breakages of SMPC cylinders by grooves of different depths. In order to better demonstrate the damage morphologies of SMPC cylinders, the grooves are compressed to 16mm to make sure the breakages of the SMPC cylinders are more significant.

5. Experiments results

5.1 Test results for SMP and SMPC plate specimens

5.1.1 DMA test results

As shown in Fig. 9(a), when the material is at low temperatures, its storage modulus maintains a relatively high value, thus it will be too stiff to deform. With the increasing in temperature, the storage modulus drops rapidly until it maintains at a relatively low value, so far, the materials will be easy to be deformed. The storage modulus of SMPC starts at 5878 MPa and ends at 143 MPa throughout the experiment, while for the SMP, its storage modulus starts at 1082 MPa and ends at 10 MPa, respectively. Therefore, the enhancement of carbon fiber is obvious. The change of storage modulus around Tg is an important feature for SMP materials. In Fig. 9(b), Tan Delta represents the tangent of phase angle between strain and stress of viscoelastic material under alternating force field, which equal to the ratio of loss modulus to storage modulus. The temperature at the highest value of Tan Delta represents the glass transition temperature of the material. Figure 9(b) indicates that the Tg of the epoxy resin and carbon fiber reinforced epoxy composite are 98℃ and 70℃, respectively. It may be caused by the following reasons:

(1) the carbon fiber cannot react with the epoxy resin, so only van der Waals force is involved in the interfacial bonding of carbon fiber and epoxy resin. Carbon fiber has a weak bonding effect on the chain motion of epoxy resin, therefore, the molecules of matrix resin can move more easily, which may cause a decrease of Tg.

(2) What's more, the thermal conductivity of carbon is much better than that of epoxy resin, so, with the addition of carbon fiber, the thermal conductivity of the materials is improved. Therefore, the Tg of SMPC is lower than that of SMP.

The DMA test curves (Figure 9) show the effect of the reinforcement by carbon fiber distinctly. The carbon fiber reinforcement increased the storage modulus significantly but lowered the Tg of the epoxy resin.

5.1.2 Static mechanical test results

As shown in Fig. 10, the tensile moduli of epoxy-based SMP specimens under 25℃, 60℃, 80℃, 100℃, and 120℃ are 1800MPa, 670MPa, 18.8MPa, 13.9MPa and 12.2MPa, respectively, while the tensile strength are 65.4MPa, 19.5MPa, 15.3MPa, 3.3MPa and 1.5MPa, respectively. The tensile modulus and strength both decrease with the increasing in temperature, this regularity is similar with that of the storage modulus. Figure 10 also shows that the tensile moduli of the SMPC under 25℃, 60℃, 80℃, 100℃, and 120℃ are 2175MPa, 1035MPa, 115MPa, 81MPa and 79MPa, respectively, while the tensile strength are 134MPa, 115.4MPa, 113MPa, 69.8MPa and 50MPa, respectively. Similar with the tensile modulus and tensile strength of SMP, the tensile modulus and strength of SMPC are also sensitive to temperature and have the same variation tendency. Because of the reinforcement of carbon fibers, the SMPCs have a higher tensile modulus and strength compared with the pure SMP, especially at high temperature. Therefore, carbon fibers can effectively enhance the mechanical properties for the epoxy-based SMP.

In addition to modulus and strength, the toughness is also a key performance to evaluate the mechanical properties of materials. Elongation at break under different temperature is measured to determine the toughness of the epoxy-based SMP and SMPC specimens. As temperatures rise (25℃, 60℃, 80℃, 100℃, and 120℃), the elongations at break of SMP specimens offer earlier increase and later decrease trend, which are 9.89%, 22.65%, 65.5%, 24.8% and 10.6%, respectively, as shown in Fig. 11.

As for the SMPC specimens, the elongations at break are much lower, which are only 1.5%, 4.3%, 7.2%, 8.2%, 4.5%, respectively. The main reason for this phenomenon is that the carbon fiber is a kind of fragile material, so, the material may become more brittle with the addition of carbon fiber. When the temperature is 80℃ and 100℃, the epoxy-based SMP and SMPC has the best toughness to withstand greater deformation, respectively.

5.1.3 Shape memory property test results

Figure 12 presents the shape fixed and recovery process of the shape memory epoxy resin. As read from the figure, the θ_{fixed}, θ_{re} and t_{re} are 3°, 0° and 10s, respectively. After calculation, the shape retention ratio and shape recovery ratio for the SMP are 98.3% and 100%, respectively, while the shape recovery rate is 17.7°/s. When carbon fiber is added as the reinforcement, the shape memory performance doesn't decline, even slightly enhance, as shown in Fig. 13. After calculation, the shape retention ratio and shape recovery ratio for the SMPC are both 100% approximately, while the shape recovery rate is 22.5°/s. Both the epoxy-based SMP and its composite can achieve close to 100% shape retention ratio and shape recovery ratio, so that the shape memory properties are excellent. Meanwhile, the shape recovery rate for this material is fast, therefore, the actuation duration for devices which are made by this kind of shape memory materials would be shorter.

6.2 Characterizations of the SMP/SMPC smart releasing devices

6.2.1 Locking compression test results

Figure 14 presents the compressive force-displacement response of devices with and without the inner core. Compared the two curves in Fig. 14, when the SMPC cylinder was compressed without the inner cylinder, the compressive force increased linearly and slowly. However, if the SMPC cylinder was assembled and fixed together with the inner core, the compressive curve rocketed when the SMPC cylinder was compacted with the inner core's grooves, and this depth was determined to be about 12mm. Therefore, when investigating the relationship between groove's depth and locking force of the SRD, 10mm, 12mm and 14mm are appropriate choices.

6.2.2 Axial tensile test results

As shown in Fig. 15, the SRD SMP2-14 has worse carrying capacity of 1311N compared with the SMPC2-14 cylinders, which may not be able to provide sufficient locking force. Furthermore, the carrying load-displacement curve increases almost linearly and then it goes done abruptly. The cause of this phenomenon is that the epoxy-based SMP is a kind of fragile material, the SMP device will suffer destruction when the tensile load beyond its carrying capacity. To overcome this defect, carbon fiber is used as a reinforcing material. The carrying capacities of the SMPC devices with 1, 2, 3 grooves, which are 14 mm deep can also be seen in Fig. 15. The load-bearing capacities of the releasing device (SMPC1-14, SMPC2-14, SMPC3-14) are 1979N, 2812N and 4327N, respectively. The tensile load of the device increased rapidly in the beginning, while with the increase of the relative displacement, the curves gradually flatten. This phenomenon may be caused by the swelling of the SMPC grooves with the process of the tensile experiment. In the beginning of the test, the SMPC cylinder

is locked tightly with the inner core, there is almost no relative displacement between the SMPC cylinder and the inner core, so the displacement may be caused by the deformation of the SMPC cylinder. With the increase of the tensile load, the SMPC grooves gradually been stretched and relative sliding occur. The force which is required to deform the SMPC grooves is much larger than that of the sliding friction between the SMPC cylinder and the inner core. So, the maximum load points represent the beginning of the relative sliding of the devices. When the depth of the grooves is 14mm, no matter how many grooves the devices have, the maximum load points always happen when devices are elongated about 2.5mm, which is within the allowable range.

Besides, the carrying capacities of the SMPC SRDs with 10mm and 12mm deep grooves, of which the number is two are also considered. The loads of the releasing devices (SMPC2-10, SMPC2-12) are 1115N and 1966N, respectively. With the decreasing of depth, the load of the releasing device attenuates obviously. Although the depth of grooves decreases 14% compared with the SMPC2-14, the maximum load reduces 30%, even lower than that of the device SMP2-14. What's more, with the decreasing of groove's depth, the SMPC cylinder is not too tightly locked with the inner core, relative displacement between the SMPC cylinder and the inner core occurs in the beginning of the test. There is sliding friction between the outer cylinder and the inner core at the beginning of the test, therefore the load increases relatively slowly at the very start. Based on the design of grooves, it can satisfy the demands of different carrying capacities.

6.2.3 Relaxation test results

Figure 16 shows the relaxation test results of the SMPC releasing devices with 1, 2, 3 pairs of grooves (SMPC1-14, SMPC2-14, SMPC3-14). A test condition of 1000N is chosen to be the initial tensile force for the experiment. Firstly, 1000N initial axial tensile force was applied to the device, then the relative displacement remained unchanged, meanwhile the axial tensile force was recorded during the test period (24 hours).

As shown in Fig. 16, the locking load dropped rapidly at the beginning of the relaxation test, but as time went by, the decreasing tendency became more and more gentle until it almost became unchanged. After 24 hours, the remaining locking loads of the devices SMPC1-14, SMPC2-14, SMPC3-14 dropped 41%, 27%, 16%, respectively. What' more, when the experiment lasted only 10 hours, the load-carrying capacity of the device SMPC3-14 became almost unchanged, while this time for the device SMPC2-14 increased to 15 hours. But even when the experiment was done, the load-carrying capacity of the device SMPC1-14 was still falling. In comparison of the three groups of experiments, with the increase of the grooves, the residue locking force of the device will remain more, and the device will become stable more easily. So, in dimensions permitting, increasing the number of the grooves is benefit for the safety of the releasing device.

6.2.4 Recovery test results of the smart releasing device

Figure 17 and Figure 18 show the whole releasing process of the SMPC cylinder and the SRD. A recorded time 22s is needed to complete the deformation recovery process of the SMPC cylinder with a pair of 14mm deep grooves, as shown in Figure

17. In the same way, the recovery time of SMPC1-14 is 28s as shown in Fig. 18, after that, the outer cylinder will completely restore and only a very small external force is needed to achieve the releasing. In order to eliminate gravity effect, the SMPC1-14 is placed horizontally and vertically to test the recovery time, and the recovery time are the same.

6.2.5 Morphology before and after releasing

Figure 19 reveals the morphologies of SMPC cylinders before and after releasing with different deep grooves. When the SMPC cylinders are subjected to varying degrees of compression, different kinds of damages may occur. When grooves are 10mm and 12mm deep, there are no macro-morphological damages as shown in Fig. 19(a). However, as shown in the SEM photograph, there are some differences in the micro-morphologies. The carbon fibers of 10mm deep groove still maintain integrity, which means that there is almost no damage in the process of locking and releasing, while when the grooves are 12mm, some fiber fractures will occur. When the grooves are 14mm deep, slightly delamination can be observed from both the macro-morphologies and micro-morphologies, but the load-bearing capacity of the device is still high, as mentioned in 4.2.2. When the depth of grooves increases to 16mm, catastrophic structural failure will occur, and the device will lose its carrying capacity.

7. Conclusions

This paper presents a kind of shockless smart leasing device based on shape memory polymer composites. Various shapes of the active element are compared to achieve a high load capacity in locked state, and the sandglass-like shape is superior in terms of carrying capacity. The critical elements of the releasing mechanism are outer part and inner part. The SMP or SMPCs active element is the outer part, while the inner part is a sandglass-like profile. The volume fraction of the carbon-fibers of SMPCs is 60%, and the winding angle is 45°. In the locked state, the outer part is sandglass-like, the outer part and the inner part are closely combined, so that the smart releasing device can bear the axial tensile force. When the outer part is heated again, it will recover its initial cylinder-shape, and the device can release easily. This type of smart leasing device has the advantages of being simple-structure, high-reliability, and the ability to carry big load, which can be more than 4000N. From the axial tension and the relaxation tests, there are obvious regularities that with the increase of the number of grooves, the load-bearing capacities and the remaining locking loads of the smart leasing device will increase distinctly, so that the device will be more stable and reliable. The depth of grooves also has a significant influence on carrying capacities of the devices. With the increase of the groove's depth of the cylinder, the structure carrying capacity of the smart leasing device increases obviously, but there will appear damage on the surface of SMPCs cylinder. With the increase of groove's depth, the damage will be more serious. Therefore, the size of the smart leasing device can be reasonably configured according to demand via the design of the groove's depth and number. The deformation recovery time of SMPCs cylinder is 22s while the releasing time for the releasing device is 28s.

Acknowledgement

This work is supported by the SAST Foundation (Grant No. SAST2016055), National Natural Science Foundation of China (Grant No. 11632005, 11672086), Joint Fund Project of National Natural Science Foundation of China (Grant No. U1637207)

References

[1] Sun J, Liu Y, Leng J. Mechanical properties of shape memory polymer composites enhanced by elastic fibers and their application in variable stiffness morphing skins. J Inte Mater Syst Struct. 2014; 26: 2020-27.

[2] Tobushi H, Hara H, Yamada E, Hayashi S. Thermomechanical properties in a thin film of shape memory polymer of polyurethane series. Smart Mater Struct. 1996; 5: 483-91.

[3] Li F, Zhu W, Zhang X, Zhao C, Xu M. Shape memory effect of ethylene–vinyl acetate copolymers. J Appl Polym Sci. 2015; 71: 1063-70.

[4] Liu T, Zhou T, Yao Y, Zhang F, Liu L, Liu Y, et al. Stimulus methods of Multi-functional Shape Memory Polymer Nanocomposites: A review. Compos Part A-Appl S. 2017; 100: 20-30.

[5] Bouaziz R, Roger F, Prashantha K. Thermo-mechanical modeling of semi-crystalline thermoplastic shape memory polymer under large strain. Smart Mater Struct. 2017; 26.

[6] Hu J, Chen W, Fan P, Gao J, Fang G, Cao Z, et al. Uniaxial tensile tests and dynamic mechanical analysis of satin weave reinforced epoxy shape memory polymer composite. Polym Test. 2017; 64: 235-41.

[7] Shen D, Shi S, Xu T. Effects of two-dimensional programming on microstructures and thermal properties of shape memory polymer-based composites: Article. J Appl Polym Sci. 2017; 134.

[8] Parvin A, Raad J. Internal and External Reinforcement of Concrete Members by Use of Shape Memory Alloy and Fiber Reinforced Polymers under Cyclic Loading-A Review. Polymers-Basel. 2018; 10: 376.

[9] Razavilar R, Fathi A, Dardel M, Hadi JA. Dynamic analysis of a shape memory alloy beam with pseudo elastic behavior. J Intel Mater Syst Struct. 2018: 1045389X-1775426X.

[10] Guo X, Liu L, Liu Y, Zhou B, Leng J. Constitutive model for a stress- and thermal-induced phase transition in a shape memory polymer. Smart Mater Struct. 2014; 23: 105019.

[11] Wu R, Han MW, Lee GY, Ahn SH. Woven type smart soft composite beam with in-plane shape retention. Smart Mater Struct. 2013; 22: 5007.

[12] Maji AK, Starnes MA. Shape measurement and control of deployable membrane structures. Exp Mech. 2000; 40: 154-9.

[13] Tan Q, Liu L, Liu Y, Leng J. Thermal mechanical constitutive model of fiber reinforced shape memory polymer composite: Based on bridging model. Compos Part A-Appl S. 2014; 64: 132-8.

[14] Yu K, Liu Y, Leng J. Shape memory polymer/CNT composites and their microwave induced shape memory behaviors. RSC Adv. 2013; 4: 2961-8.

[15] Tobushi H, Okumura K, Hayashi S, Ito N. Thermomechanical constitutive model of shape memory polymer. Mech Mater. 2001; 33: 545-54.

[16] Behl M, Razzaq MY, Lendlein A. Multifunctional shape-memory polymers. Adv Mater. 2010; 22: 3388-3410.

[17] Kodama M, Karino I, Kobayashi J. Interaction between the reinforcement and matrix in carbon-fiber-reinforced composite: Effect of forming the thin layer of polyimide resin on carbon fiber by in situ polymerization. J Appl Polym Sci. 2010; 33: 361-73.

[18] Zhang CS, Ni QQ. Bending behavior of shape memory polymer-based laminates. Compos Struct. 2007; 78: 153-61.

[19] Liu Y, Lv H, Lan X, Leng J, Du S. Review of electro-active shape-memory polymer composite.

Compos Sci Tech. 2009; 69: 2064-8.
[20] Liu C, Qin H, Mather PT. Review of progress in shape-memory polymers. J Mater Chem. 2007; 17: 1543-58.
[21] Liu Y, Du H, Liu L, Leng J. Shape memory polymers and their composites in aerospace applications: a review. Smart Mater Struct. 2014; 23: 23001-22.
[22] Kim BK, Sang YL, Mao X. Polyurethanes having shape memory effects. Polymers-Basel. 1998; 37: 5781-93.
[23] Qiao T, Liu L, Liu Y, Leng J. Post buckling analysis of the shape memory polymer composite laminate bonded with alloy film. Compos Part B-Eng. 2013; 53: 218-25.
[24] Guo X, Liu L, Zhou B, Liu Y, Leng J. Constitutive model for shape memory polymer based on the viscoelasticity and phase transition theories. J Intel Mater Syst Struct. 2016; 27: 314-23.
[25] Guo J, Liu J, Wang Z, He X, Hu L, Tong L, et al. A thermodynamics viscoelastic constitutive model for shape memory polymers. J Alloy Compo. 2017; 705: 146-55.
[26] Fosness E, Peffer A, Denoyer K. Overview of Spacecraft Deployment and Release Devices Efforts at the Air Force Research Laboratory. American Society of Civil Engineers. 2000: 312-8.
[27] Leng J, Lan X, Liu Y, Du S. Shape-memory polymers and their composites: Stimulus methods and applications. Prog Mater Sci. 2011; 56: 1077-135.
[28] Hornbogen E. Review Thermo-mechanical fatigue of shape memory alloys. J Mater Sci. 2004; 39: 385-99.
[29] Huang W, Toh W. Training two-way shape memory alloy by reheat treatment. J Mater Sci Lett. 2000; 19: 1549-50.
[30] Yang BJ, Wang ZW, Gai YX. Research Progress of Non-Pyrotechnic Releasing Devices on the Spacecraft. Machinery Design and Manufacture. 2018.
[31] Mccloskey TE. Non-pyrotechnic release system. 1993.
[32] Roshan U, Amarasinghe R, Nanayakkara ND. Design and Development of a Shape Memory Alloy Spring Actuated Gripper for Minimally Invasive Surgeries. International Conference on Artificial Life and Robotics. 2018.
[33] Gao B. Shape Memory Alloys and Their Application to Aerospace Separation Mechanisms. Spacecraft Recovery and Remote Sensing. 2005.
[34] Wei H, Guan C, Du H, Liu L, Leng J.A new release device based on styrene-based SMP reinforced by carbon fiber. Proceedings of SPIE - The International Society for Optical Engineering . 2013; 8793: 4215-27.
[35] Pretsch T. Review on the Functional Determinants and Durability of Shape Memory Polymers. Polymers-Basel. 2010; 2: 120-58.
[36] Gall K, Lake M, Harvey J, Ricca E. Development of a Shockless Thermally Actuated Release Nut Using Elastic Memory Composite Material. AIAA J. 2013.
[37] Wei H, Liu L, Zhang Z, Du H, Liu Y, Leng J. Design and Analysis of Smart Release Devices Based on Shape Memory Polymer Composites. Compos Struct. 2015; 133: 642-51.
[38] Revathi A, Murugan MS, Rao S, Chiranjeevi MC, Rao KV, Srihari S, et al. Investigations on tensile creep of CNT-epoxy shape memory polymer nanocomposites. Int J Nanotechn. 2017; 14: 945.
[39] Mcclung A, Tandon G, Baur J. Effects of Loading Rate on the Relaxation and Recovery Ability of an Epoxy-Based Shape Memory Polymer. Fluids. 2017; 2: 13.
[40] Hu J, Chen W, Fan P, Gao J, Fang G, Cao Z, et al. Epoxy shape memory polymer (SMP):

Material preparation, uniaxial tensile tests and dynamic mechanical analysis. Polymer Test. 2017; 62: 335-41.
[41] Gramoll K. Stress analysis of filament wound open-ended composite shells. Proc. of the 34th Structure, Structural Dynamics, and Materials (SDM) Conf. 1993.
[42] Fukunaga H and Chou T W. On laminate configurations for simultaneous failure. Journal of Composite Materials, 1988; 22: 271- 86.
[43] Fukunaga H and Chou T W. Simplified design techniques for laminated cylindrical pressure vessels under stiffness and strength constraints. Journal of Composite Materials, 1988; 22: 1156-69.
[44] Giles G L. Design-oriented analysis of aircraft fuselage structures using equivalent plate methodology. Journal of Aircraft, 1999; 36(11): 21-8.
[45] Leng J, Lan X, Du S. Shape Memory Polymer and Multifunctional Nanocomposite, CRC Press/ Taylor & Francis. 2010.
[46] Lan X, Wang X, Liu Y, Leng J. Fiber reinforced shape-memory polymer composite and its application in a deployable hinge. Smart Mater Struct. 2009, 18: 024002.
[47] Leng J, Lan X, Liu Y, Du S. Shape memory polymer composites and their applications in space deployable structures. Chinese J Aero. 2010, 31: 950-6.

Figure Captions

Fig. 1. Schematic illustration of the working procedure of the smart locking and releasing device: (a) fixing the outer cylinder and inner cylinder. (b) heating the smart releasing device. (c) pre-deforming the smart releasing device by compression clamp. (d) the locking state of the smart releasing device. (e) the releasing state of the smart releasing device. (f) a kind of heating strategy.

Fig. 2. Smart releasing device made by SMP and SMPC. (a) The inner core of the smart releasing device made by stainless steel, (b) The outer core of epoxy resin SMP cylinder, (c) The SMP smart releasing device, (d) The outer core of carbon fiber reinforced SMPC cylinder, (e) The SMPC smart releasing device.

Fig. 3. The simplified SMPC cylinder

Fig. 4. The typical geometrical shape and coordinate system of SMPC cylinder

Fig. 5. Analysis result of the theoretical model

Fig. 6. Design of the mould of the SMP cylinder

Fig. 7. The schematic diagram of shape fixed and recovery process of the shape memory epoxy resin.

Fig. 8. (a) Axial tensile test of the SRD. (b) Locking compression test of the SRD. (c) Relaxation test of the SRD.

Fig. 9. DMA test result of SMP and SMPC. (a) Storage modulus of SMP and SMPC. (b) Tg of SMP and SMPC.

Fig. 10. Tensile modulus-temperature and tensile strength- temperature relations of pure shape memory epoxy resin and its composite.

Fig. 11. Elongation at break-temperature relations of pure shape memory epoxy resin.

Fig. 12. The shape memory process of pure epoxy resin.

Fig. 13. The shape memory process of carbon fiber reinforced epoxy resin composite.

Fig. 14. Tensile force-displacement relations of the SRD with or with the inner cylinde

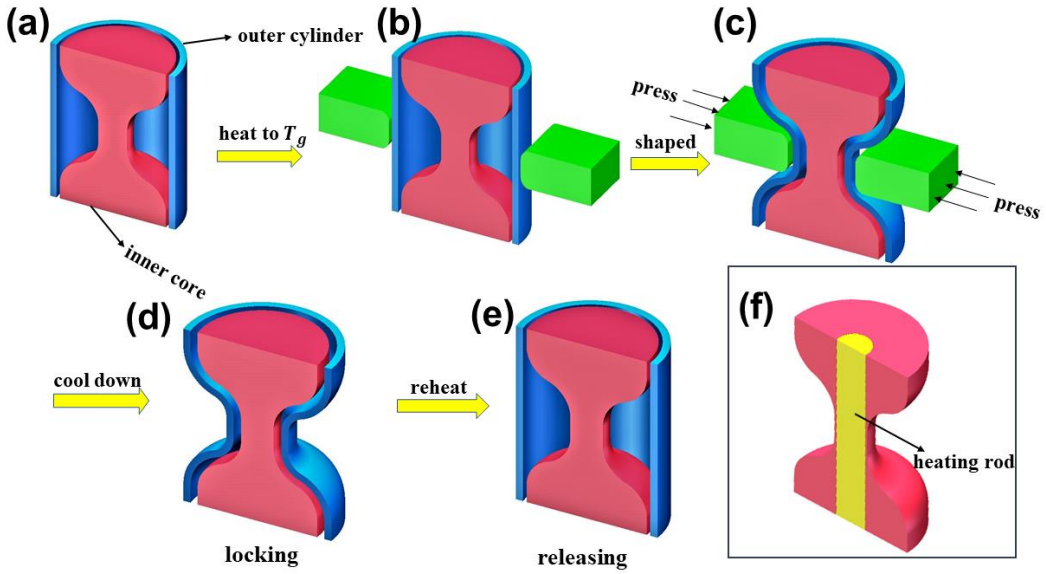

Fig. 1. Schematic illustration of the working procedure of the smart locking and releasing device: (a) fixing the outer cylinder and inner cylinder. (b) heating the smart releasing device. (c) pre-deforming the smart releasing device by compression clamp. (d) the locking state of the smart releasing device. (e) the releasing state of the smart releasing device. (f) a kind of heating strategy.

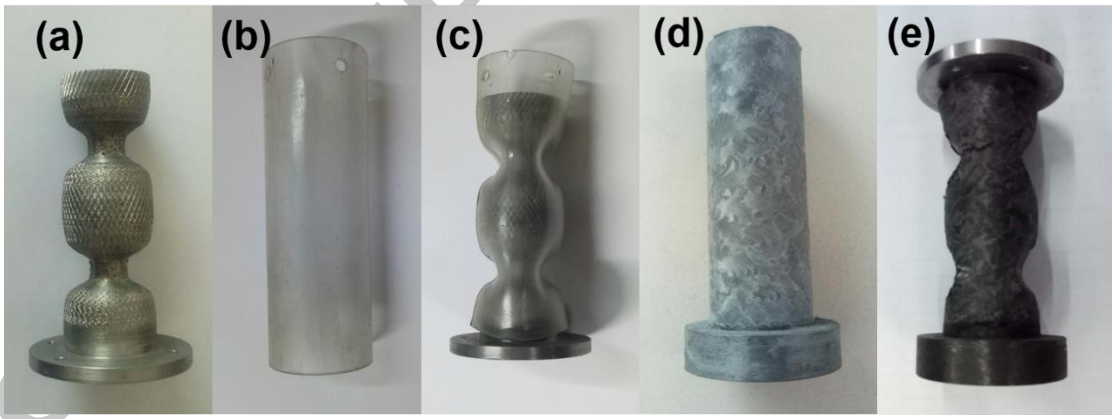

Fig. 2. Smart releasing device made by SMP and SMPC. (a) The inner core of the smart releasing device made by stainless steel, (b) The outer core of epoxy resin SMP cylinder, (c) The SMP smart releasing device, (d) The outer core of carbon fiber reinforced SMPC cylinder, (e) The SMPC smart releasing device.

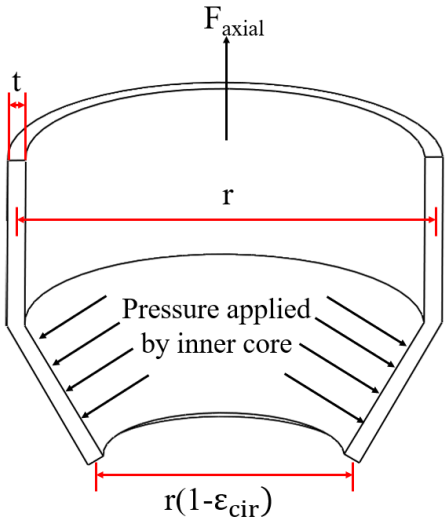

Fig. 3. The simplified SMPC cylinder

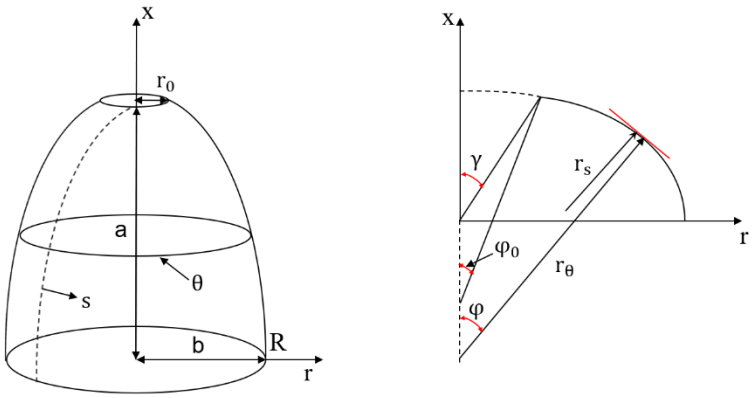

Fig. 4. The typical geometrical shape and coordinate system of SMPC cylinder

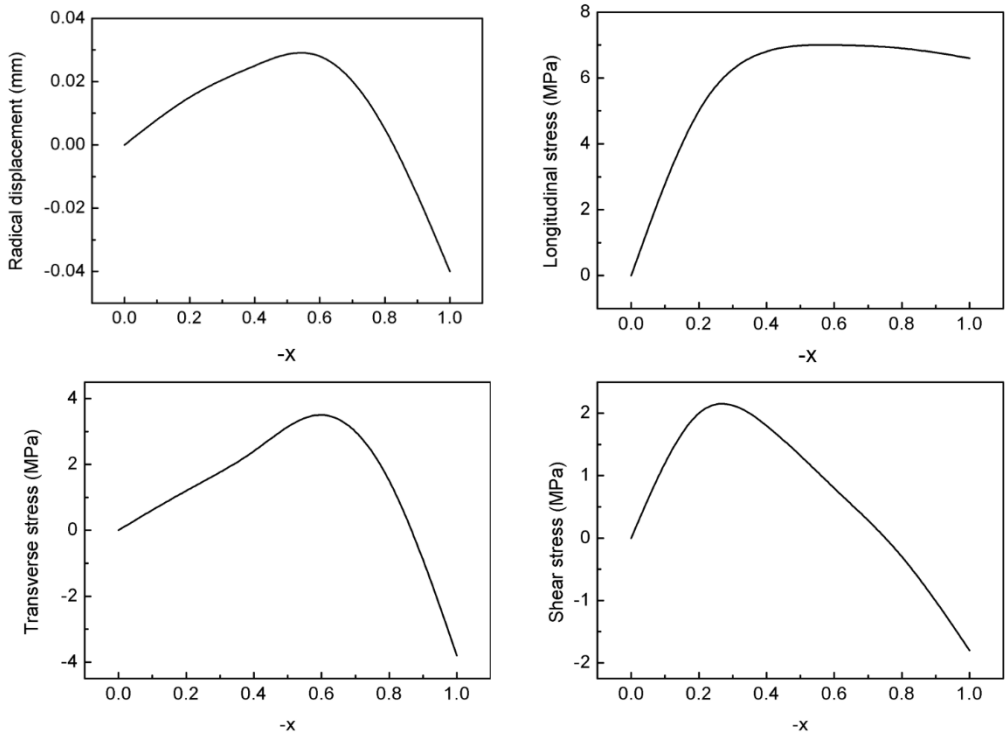

Fig. 5. Analysis result of the theoretical model

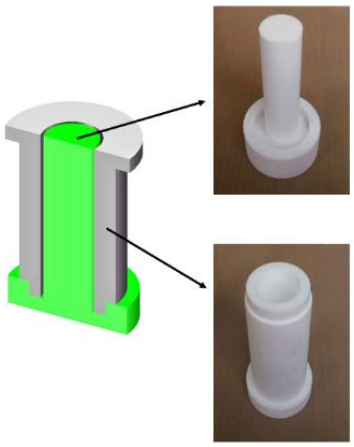

Fig. 6. Design of the mould of the SMP cylinder

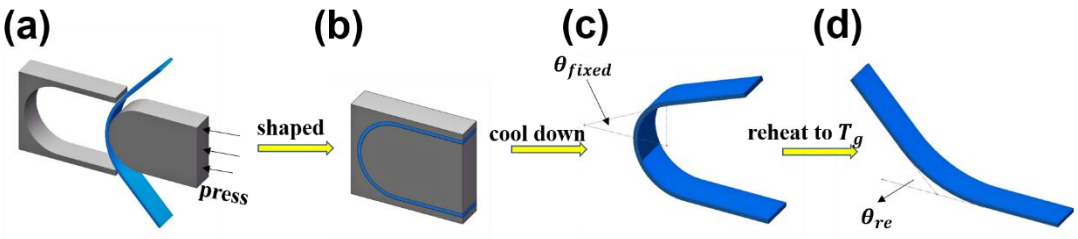

Fig. 7. The schematic diagram of shape fixed and recovery process of the shape memory epoxy resin.

Fig. 8. (a) Axial tensile test of the SRD. (b) Locking compression test of the SRD. (c) Relaxation test of the SRD.

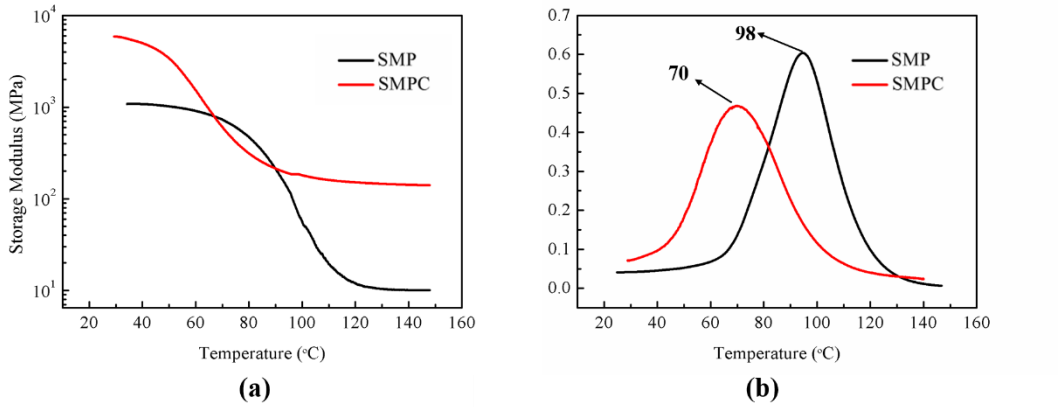

Fig. 9. DMA test result of SMP and SMPC. (a) Storage modulus of SMP and SMPC. (b) Tg of SMP and SMPC.

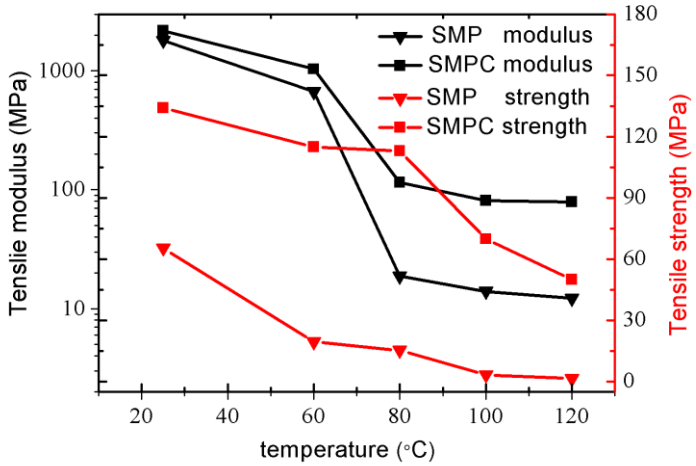

Fig. 10. Tensile modulus-temperature and tensile strength- temperature relations of pure shape memory epoxy resin and its composite.

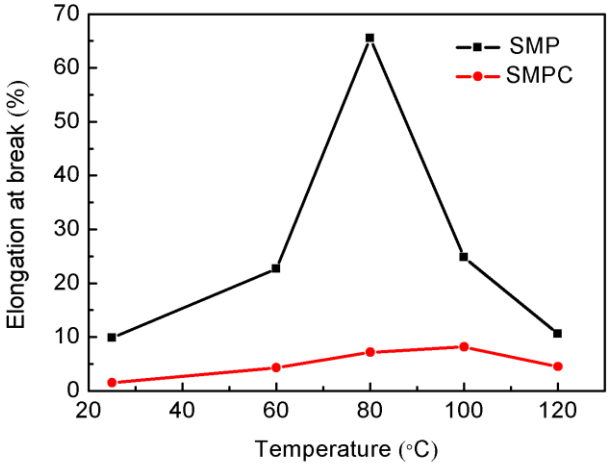

Fig. 11. Elongation at break-temperature relations of pure shape memory epoxy resin and its composite.

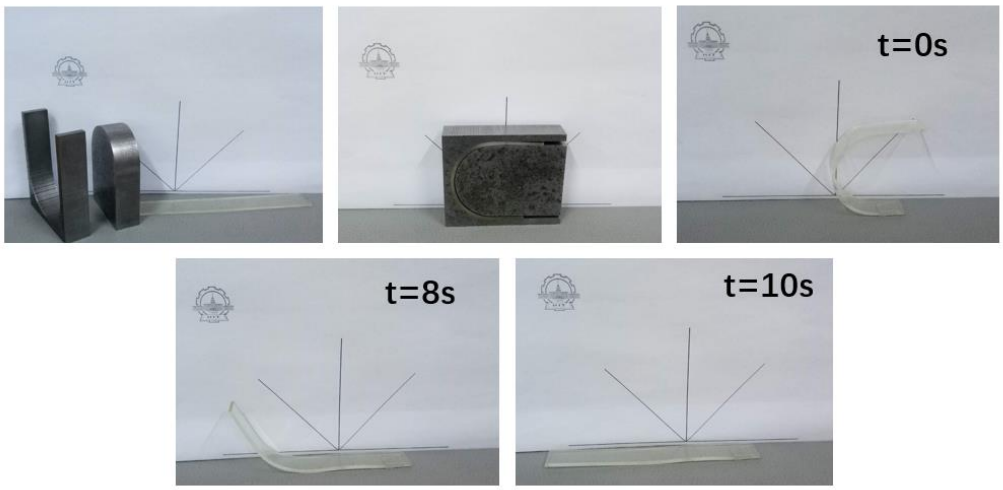

Fig. 12. The shape memory process of pure epoxy resin.

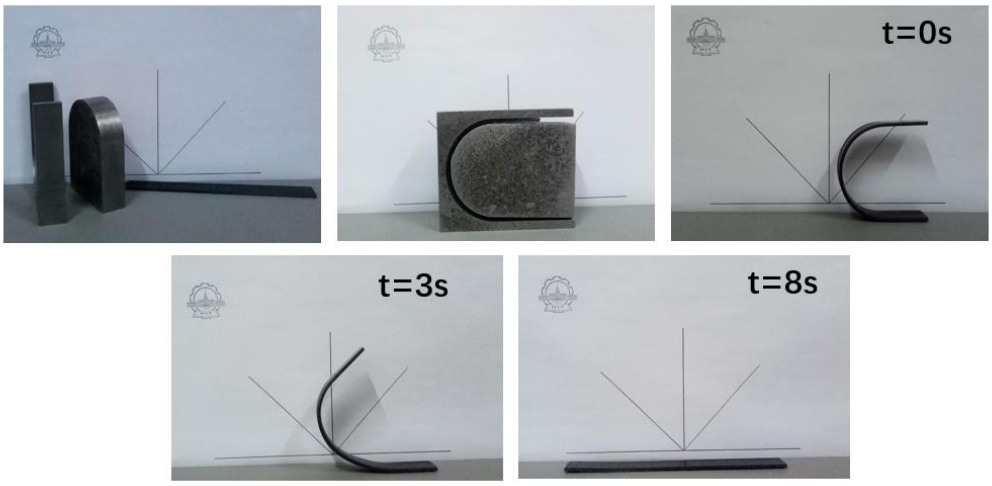

Fig. 13. The shape memory process of carbon fiber reinforced epoxy resin composite.

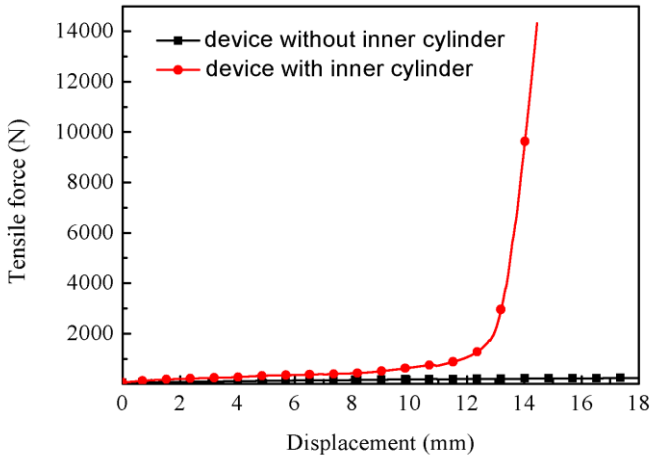

Fig. 14. Tensile force-displacement relations of the SRD with or with the inner cylinder

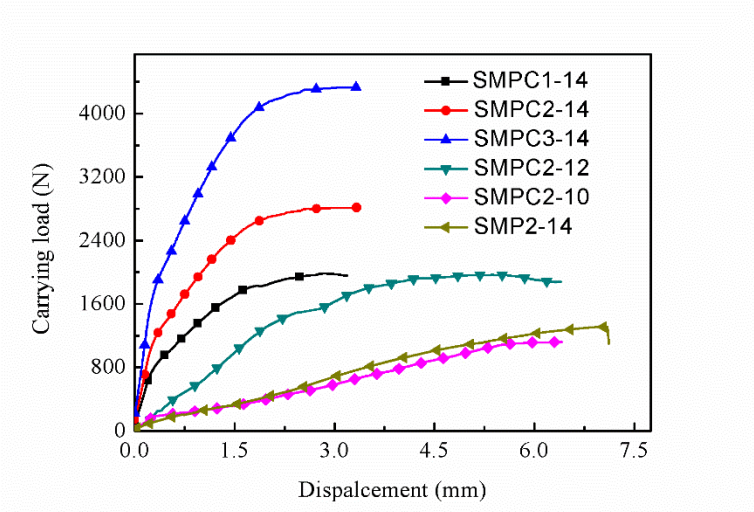

Fig. 15. The carrying load-displacement relations of SRDs under different configurations.

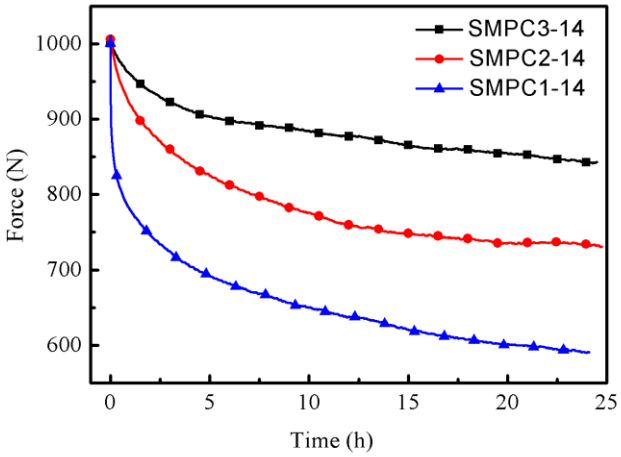

Fig. 16. Relaxation test curves of SRDs under different configurations.

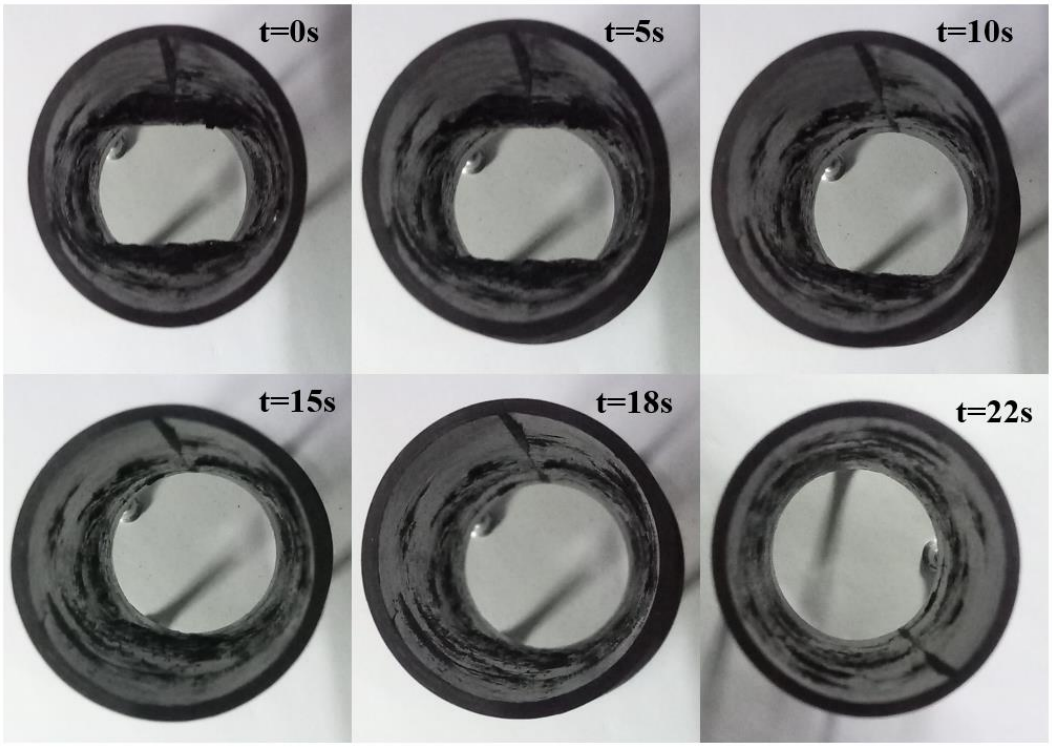

Fig. 17. Recovery test of the SMPC cylinder.

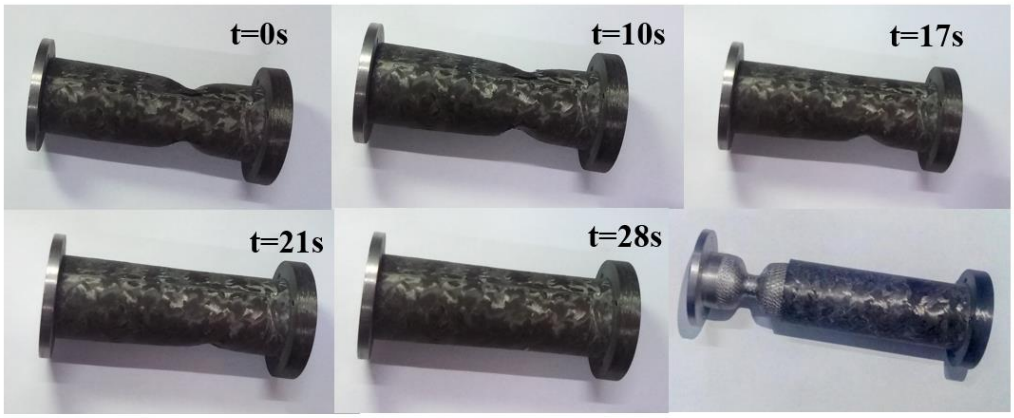

(a)

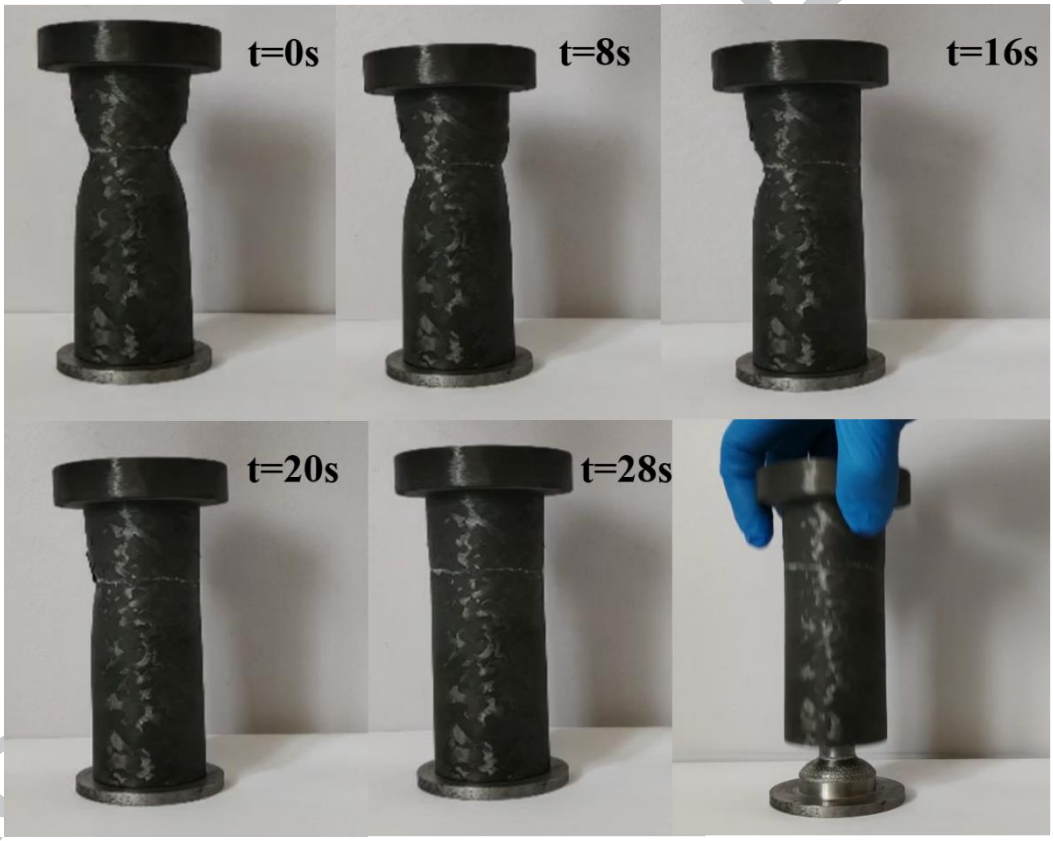

(b)

Fig. 18. Recovery test of the SRD. (a) horizontal. (b) vertical.

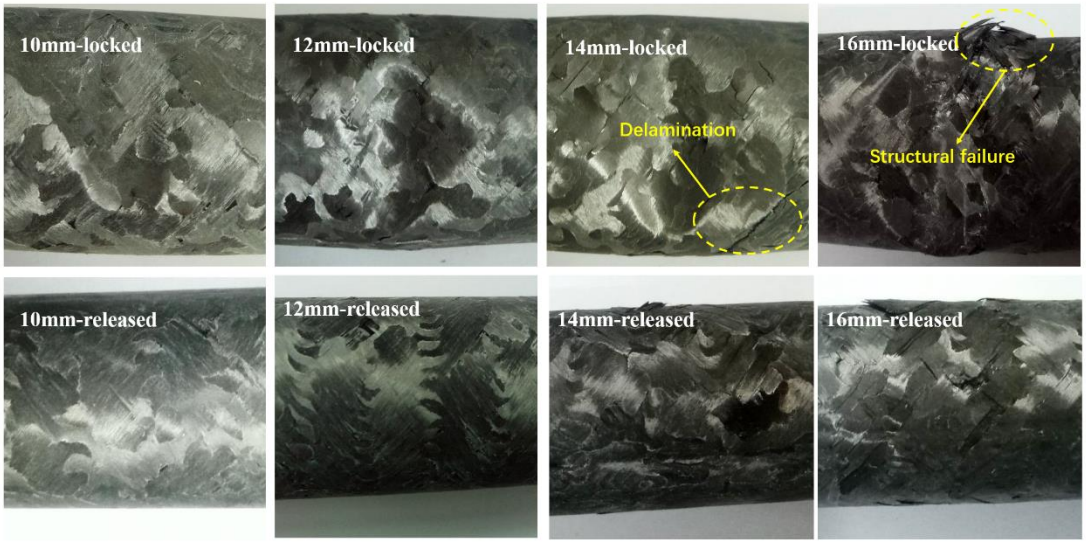

(a)

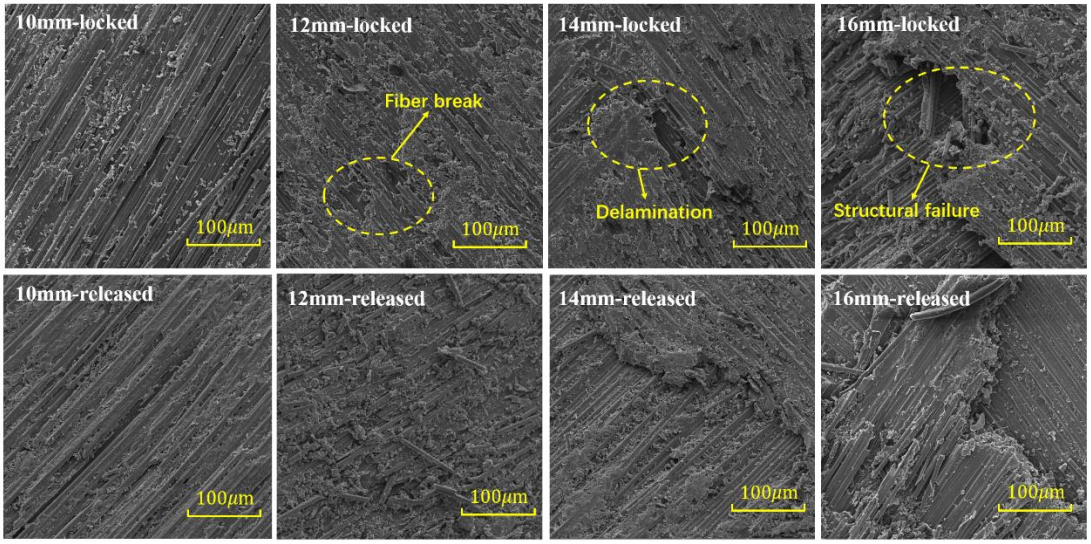

(b)

Fig. 19. Morphologies of SMPC cylinders. (a) macro-morphology. (b) micro-morphology.

Table 1
Characteristics of the SMP and SMPC cylinders.

characteristics	SMP cylinder	SMPC cylinder
Long	120mm	150mm
The inner diameter	36mm	36mm

Thickness	2mm	2mm
Material	Shape memory epoxy resin	Carbon-fiber reinforced shape memory epoxy resin

Table 2
Preliminary requirements of the SRD.

Technical indicator	Specification
Actuation time	45s
Load capacity	≥ 2500N
Transformation temperature	≥ 60℃
Recover rate	95%

Table 3
The test number of the tensile test under different conditions.

Serial number	Material of the cylinder	Number of groove	Depth of groove
SMPC1-14	SMPC	1	14mm
SMPC2-14	SMPC	2	14mm
SMPC3-14	SMPC	3	14mm
SMPC2-10	SMPC	2	10mm
SMPC2-12	SMPC	2	12mm
SMP2-14	SMP	2	14mm